Journal of Machine Construction and Maintenance
PROBLEMY EKSPLOATACJI
QUARTERLY ISSN 1232-9312 3/2017 (106)
p. 13–19

Dariusz PULIKOWSKI[*,], Friedrich LACKNER[*], Christian SCHEUERLEIN[*], Mirosław PAJOR[**]**
[*] European Organisation of Nuclear Research CERN, Geneva, Switzerland
[**] Department of Mechanical Engineering and Mechatronics, West Pomeranian University of Technology, Szczecin, Poland
dariusz.pulikowski@cern.ch

NUMERICAL MODELLING OF A SUPERCONDUCTING COIL WINDING PROCESS WITH RUTHERFORD TYPE Nb_3Sn CABLE

Key words: winding process, Rutherford cable, multibody FEA simulation, superconducting magnets.

Abstract: The upgrade of the Large Hadron Collider at CERN requires a new generation of superconducting magnets. In order to obtain very high magnetic fields, Nb_3Sn superconductors will be used. The use of this material brings new challenges to the production process of accelerator magnets for High Energy Physics application. The prototype windings of a large aperture quadrupole (MQXF) and high field two-in-one dipole (11 T) coils were performed in the Large Magnet Facility at CERN. A study was lunched in order to identify the origin of mechanical cable winding instabilities and to develop a method for further improving winding parameters. This paper focuses on a theoretical analysis of the coil winding process with use of Finite Element Method.

Modelowanie numeryczne procesu uzwajania cewek nadprzewodnikowych z użyciem przewodu Nb_3Sn typu Rutherford

Słowa kluczowe: proces uzwajania, przewód typu Rutherford, symulacja MES, magnesy nadprzewodnikowe.

Streszczenie: Modernizacja Wielkiego Zderzacza Hadronów (LHC) znajdującego się w Europejskiej Organizacji Badań Jądrowych (CERN) wymaga zastosowania nowej generacji magnesów nadprzewodnikowych. Wysokie pole magnetyczne zostanie osiągnięte przy użyciu nadprzewodnika Nb_3Sn, którego krucha struktura wiąże się z koniecznością wykorzystania techniki wind-and-react. W Zakładzie Wielkich Magnesów (LMF) przeprowadzono prototypowe uzwajanie cewek magnesu czterobiegunowego (MQXF) oraz dwubiegunowego (11 T), podczas których zaobserwowana została niestabilność mechaniczna przewodu typu Rutherford. W artykule zaprezentowano analizę teoretyczną procesu uzwajania przewodu typu Rutherford z wykorzystaniem Metody Elementów Skończonych, mającą na celu identyfikację źródła niestabilności jak i w przyszłości dostarczenie narzędzi umożliwiających optymalizację parametrów procesu.

Introduction

The Large Hadron Collider (LHC) built by the European Organization for Nuclear Research (CERN) has been operational since 2008. In the scope of the High Luminosity (HL) upgrade of the LHC and the next generation Future Circular Collider (FCC) study, new magnet production technologies are developed. The upcoming improvement requires the use of the Nb_3Sn superconductor, not yet present in any High Energy Physics (HEP) application [1]. The low-beta quadrupole (MQXF) [2] and high field two-in-one dipole (11 T) [3] magnets are designed with use of the Nb_3Sn, Rutherford type cable. The main challenge with use of the Nb_3Sn compound is its brittleness. Low intrinsic strain may cause permanent performance degradation [4]. The wind-and-react technique was developed in order to address this issue. The coil is wound with a cable in which the Nb_3Sn precursor elements are present in a common Cu matrix. The Nb_3Sn is formed in the reaction heat treatment in 650°C when the coil is in its final shape [5]. Thanks to this technique, the winding process is performed using a ductile material. In order to withstand the high temperature during reaction, S-2 glass and mica is used as the cable insulation [6].

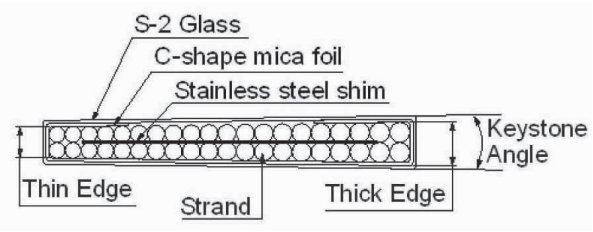

Fig. 1. Sketch of 40-Strand Rutherford cable cross-section. Pitch angle φ = 16° and strand diameter d = 0.7 mm

The superconducting strands are manufactured based on the Restacked-Rod process (RRP®). The strands (Fig. 2a) are cabled into the 40-strand cable (Fig. 2b).

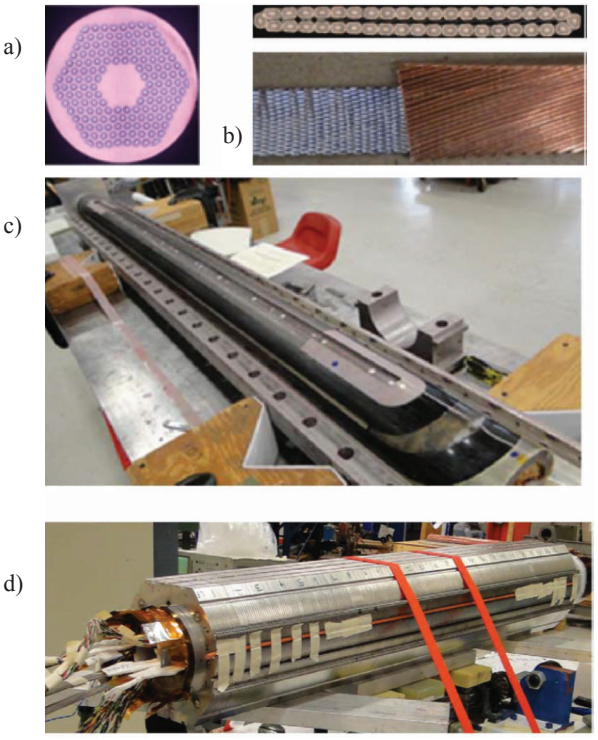

Fig. 2. a) RRP150/169 Nb_3Sn strand; b) 40-Strand stainless steel shimmed cable; c) Reacted and impregnated coil; d) Collared prototype dipole assembly

The cable is afterwards braided with S-2 glass insulation sleeve and C-shape mica foil, shown in the Fig. 3b. The wound coil is subjected to the reaction and impregnation processes (Fig. 2c). Fig. 2d shows the two-coil assembly in the dipole configuration. The prototype coil winding was performed in the Large Magnet Facility (LMF) at CERN with the use of an insulated and an uninsulated Nb_3Sn cable. The cable mechanical instabilities, like strand pop-out, protrusions, or openings, were observed [7]. In most cases, the instabilities occur at the extremities (pole-ends) of a coil. The strand pop-outs are visible in Fig. 3a as a discontinuity on the cable surface. The protrusion from the mandrel surface is shown in Fig. 3b.

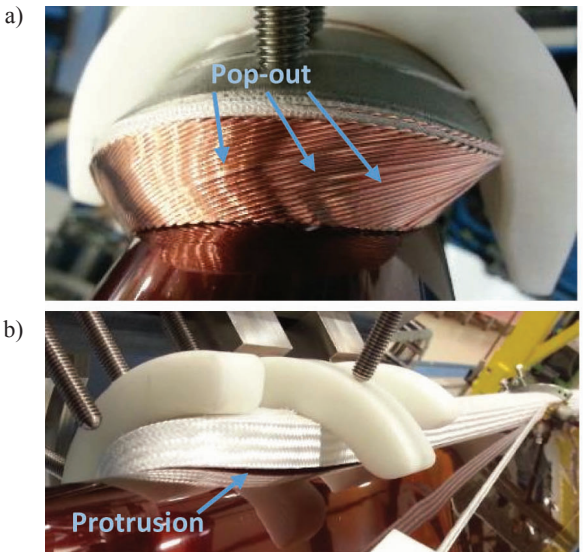

Fig. 3. Prototype coil winding with Nb_3Sn; a) Strand pop-out on pole-end; b) Right: Protrusion from a mandrel surface

In order to obtain a high and repeatable quality of the coil winding, it was crucial to identify and study the phenomena driving the cable mechanical instability by measurements and the numerical simulations. One can see that the wound cable is bent in 3-axes in order to obtain a coil shape shown in Fig. 3. The winding simulation with a Rutherford cable is simplified to 1-axis bending, with the use of a cylindrical support shown in Fig. 8. This allows for a less complex simulation setup that may be compared with the experimental results [7]. In order to investigate a relative displacement of a strand in the cable matrix, the cable is modelled with separate strand bodies. The literature describes two, three-dimensional, "hierarchical models" of the Rutherford cable, used in mechanical analysis [8] and [9], which are intended for a mechanical calculation of a filament degradation due to the applied stress. The winding simulation shown in this paper consists of a 10 mm diameter cylinder and a 20 mm-long cable. The model geometry is defined in a CAD system, allowing for an accurate mesh control.

1. Winding simulation

The support pole used in the 11 T dipole is machined from the titanium alloy, whereas the outer surface of the cable is made of copper. Due the high material stiffness difference, the cylinder is simulated as a rigid body. The plastic deformation is introduced in order to avoid the artificially high stress in the cable. The Nb_3Sn strand's material parameters are defined by the multilinear isotropic hardening property derived from the single strand tensile test performed at CERN. The result and the FEA input data is shown in Fig. 4. The elastic behaviour is described with the Young's modulus value of 90 GPa, and the used Poisson's Ratio is 0.34.

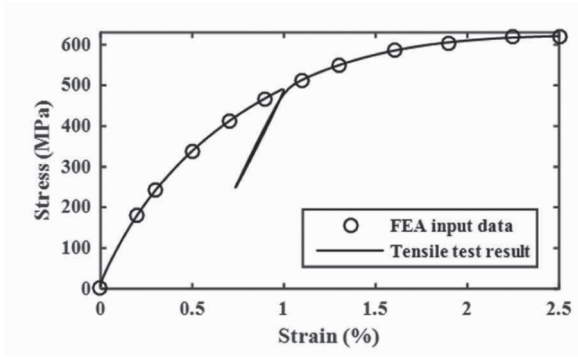

Fig. 4. Tensile test results of an Nb_3Sn 132/169 0.7 mm strand. E = 90 GPa, $\nu = 0.34$

In order to analyse the geometry of the Nb3Sn cable, a Computed Tomography (CT) of the cable stack was performed. The tomogram on the left side of Fig. 5 shows the cable stack and the transversal cross sections. One can see the plastic deformation of the initially round strands in the enlarged edges of the cable, which is caused by the cabling process [10]. The simulated strand is simplified to a round cross section, with no keystone angle. The Rutherford cable contains a stainless steel shim, which is introduced in order to increase the interstrand contact resistance [1]. The shim is a flat foil of 0.15 mm thickness. The extracted stainless steel shim visible in Fig. 2b shows multiple imprints introduced during the cabling process. The shim is considered giving negligible rigidity to the cable; therefore, it is not taken into account in the presented model.

The S-2 glass sleeve and mica C-shape foil are the outermost layers of the cable. The S-2 glass insulation is braided on the cable with a constant feed of the mica foil. The cable is tightly enclosed, which provides a mechanical support to the cable. In order to avoid the additional constraint, the insulation layers are not included in the simulated cable geometry. The geometrical simplifications of the presented model are shown in Table 1. The simulated cable geometry is presented on the right side of Fig. 5, consisting of 10 strands of 0.7 mm diameter.

Table 1. Geometrical simplifications of the simulation

Body	Feature	Simplification
Cable	Wire deformation	Not considered
	Keystone angle	Not considered
	Stainless steel shim	Not considered
	S-2 Glass and Mica insulation	Not considered
	40 strands	10 strands
Cylinder	3-axis bending	1-axis bending

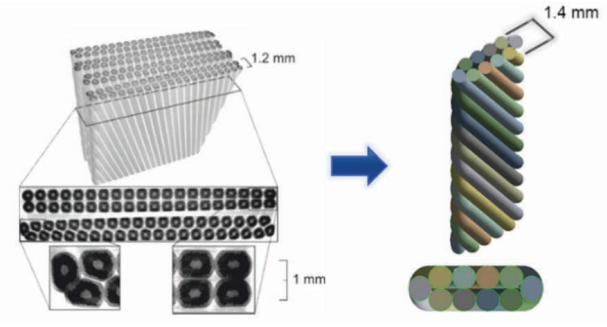

Fig. 5. Cable geometry simplification. Left: Tomography of the stack of four 40-strand Rutherford cables (from [7]). Right: FEA model of 10-strand Rutherford cable

The strand body is defined with a guide curve positioned in the centre of each strand, shown in Fig. 6. The minimal repeatable period of the cable is a turn of the strand *p*. Its value is related with a pitch angle φ and strand diameter *d* with the following equation:

$$p = \frac{d}{\sin(\varphi)} \tag{1}$$

In order to obtain the length of the cable *l* containing the full period of each strand (pitch length), the quantity of strands *n* needs to be equal to the quantity of a cable turns *p*, which is described by equation (2).

$$l = n * p \tag{2}$$

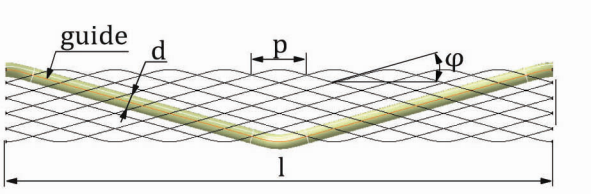

Fig. 6. Side view of the 10-Strand Rutherford cable guide curves and one strand geometry

In order to wind the 11 T dipole, it is necessary to introduce a three-axes bending to the superconductor, as shown in Fig. 3 and the left side of Fig. 8. The winding complexity is reduced to the 1-axis bending. The modelled cable is bent on the cylinder surface (right side of Fig. 8), which introduces the bending momentum in the Z-axis (Fig. 7).

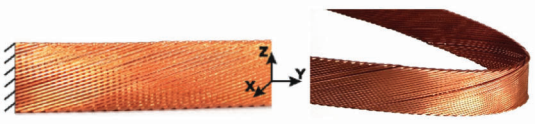

Fig. 7. Rutherford cable. Left: Bending $\overrightarrow{M} = \theta$. Right: Bending momentum in Z-axis

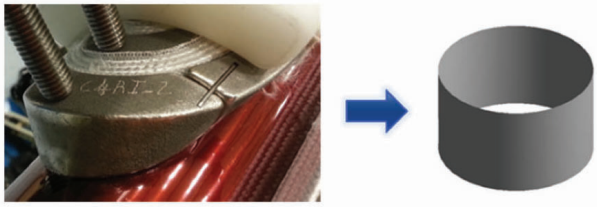

Fig. 8. Pole geometry simplification. Left: 11 T dipole end-spacer. Right: FEA winding cylinder

The winding model setup is shown in Fig. 9. The cable overall length is 25.4 mm, which presents 10 minimal periods. This configuration gives a geometry with a full period of each strand. The winding force F is defined in order to induce a turning movement of the cable around a fixed cylinder surface. The force vector has a constant value of 200 N and acts on all 10 faces of cable side B. The angle α between the force F and Y-axis is changing in the course of the simulation from 0° to 180°.

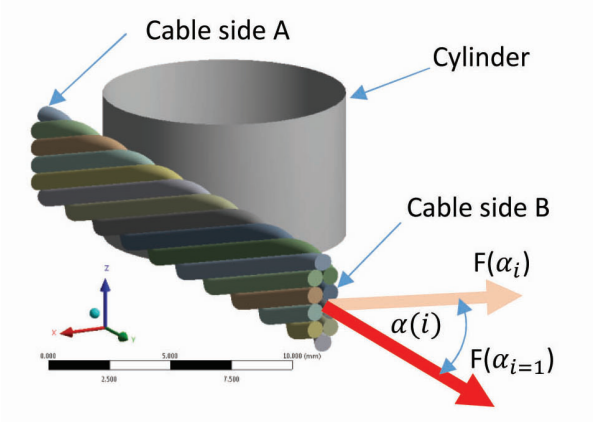

Fig. 9. The winding model setup

The boundary conditions of the model are shown in Table 2. The modelled cylinder is a rigid body fixed in 6 DOF. The strands are fixed on the side A in 6 DOF. On the side B, strands are constrained in 3 DOF, i.e. Z-translation, X-rotation, and Y-rotation. The cable boundary condition is defined with a rigid behaviour in order to eliminate the side face deformation.

Table 2. Boundary conditions

Body	Geometry	Support	Load
Strand	Face side A	Fixed 6 DOF	-
	Face side B	Fixed 3 DOF (T_Z, R_X, R_Y)	Force (200N/10)
Cylinder	Whole body	Fixed 6 DOF	-

The contact parameters of the model are presented in Table 3. The contact interfaces are defined with use of the three-dimensional 8-node contact elements, shown in Fig. 10. These elements feature the quadratic shape function, which allows for a good curved surface adjacency in the application with a coarse mesh. These elements improve the initial contact conditions by minimizing the gap and the penetration size. The friction coefficient is 0.2, which will be subject of further study. An interface between the cable faces and the cylinder is configured asymmetric, allowing for a more efficient contact analysis due to the contact force projection on the strand.

Table 3. Contact definition

Interface	Strand to strand	Strand to cylinder
Type	Frictional	Frictional
Contact element	3D 8-node	3D 8-node
Formulation	Augmented Lagrange	Augmented Lagrange
Friction coefficient	0.2	0.2
Behaviour	Symmetric	Asymmetric

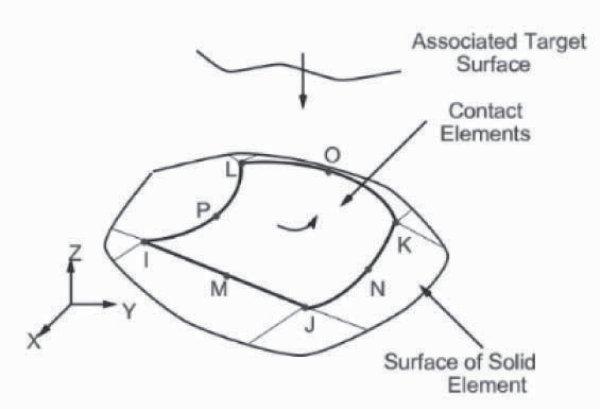

Fig. 10. 3D 8-node contact element [11]

The cable is meshed by dividing the strand geometry along the guide curve, resulting in a good mesh quality ratio, as shown in Fig. 11. The obtained longitudinal sections are divided further with use of the edge-sizing feature.

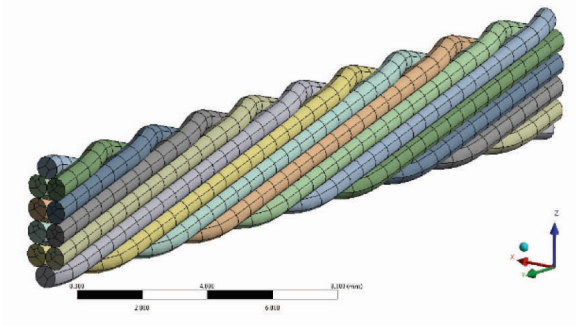

Fig. 11. The modelled cable mesh

The model was discretized with use of 20-node 3-D solid quadratic elements presented in Fig. 12. These elements allow for a good representation of a complex surface geometry.

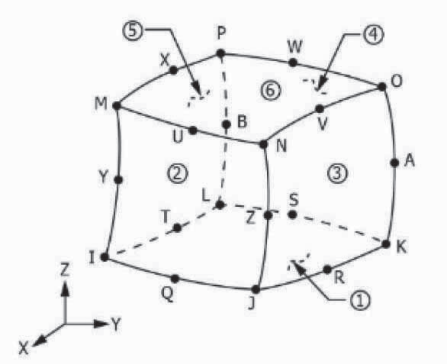

Fig. 12. 3-D 20-node quadratic solid element [11]

2. Winding simulation results and interpretation

The model deformation is shown in five steps in Fig. 13. The simulated cable geometry is characterized by the following parameters: the pitch angle $\varphi = 16°$, strand diameter $d = 0.7$ mm, and the turn distance $p = 2.54$ mm.

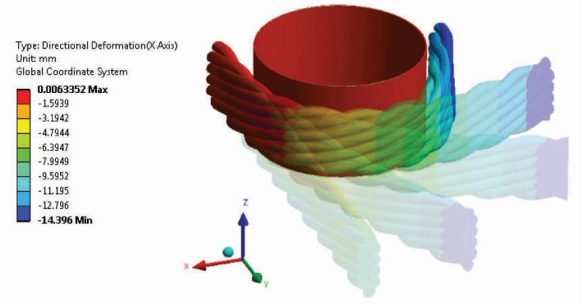

Fig. 13. Winding simulation in five steps. The result of the directional deformation in X-axis (mm)

The equivalent total strain of a final step of a simulation is presented in Fig. 14. One can see the highest strain concentration of approximately 9% close to the edges of the cable.

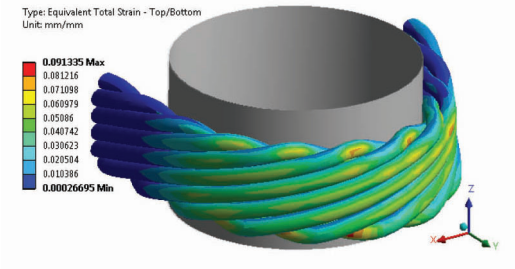

Fig. 14. Winding simulation result, Equivalent Total Strain (mm/mm)

The directional deformation in the Z-axis is shown in Fig. 15. One can see the strands in the central area of the cable protrude downwards in the Z-axis direction. The maximal absolute value of the cable protrusion is 0.61 mm, which is 87% of the strand diameter.

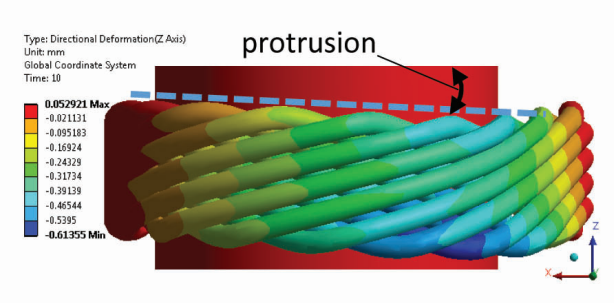

Fig. 15. The directional displacement in Z-axis with marked protrusion (mm)

The strand pop-out instability was investigated by calculating the strand distance from the centre axis of the cylinder, shown in Fig. 16. One can see that the wound strands are not equally distanced from the centre. The maximal difference is 0.1 mm, which is 15% of the strand diameter.

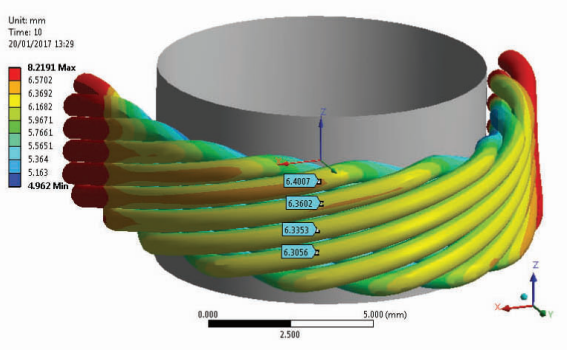

Fig. 16. Distance from the cylinder centre (mm). Strand pop-out result

The results presented in Fig. 15 and Fig. 16 lack the information of the cable position in which the deformation occurs. This is crucial when considering the comparison with the experimental results [7]. It was essential to develop an algorithm in order to extract the results in a function of an initial cable position.

4. Result analysis algorithm

The results in Fig. 17 show the position of the strands, represented by the guide curves. Each strand is represented by the function of the initial position and the displacement of an associated finite element. Such a data presentation allows one to distinguish strands easily.

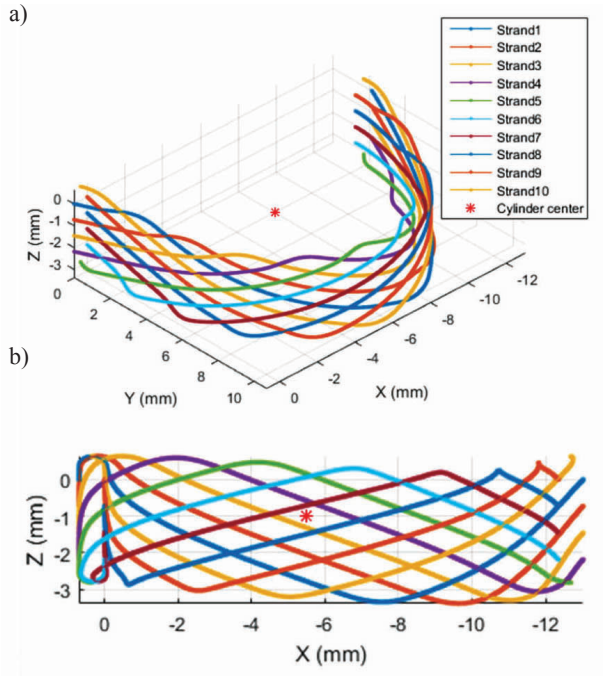

Fig. 17. Guide curve position of 10 simulated strands (mm): a) Isometric view. b) X-Z plane view

The average, maximal, and minimal directional displacement in X, Y, and Z-axes are shown in Fig. 18. One can see the protrusion phenomena as the displacement in the Z-axis. The maximal protrusion value equals 0.6 mm, which is 86% of a strand diameter occurring in 16.8 mm of the initial cable length.

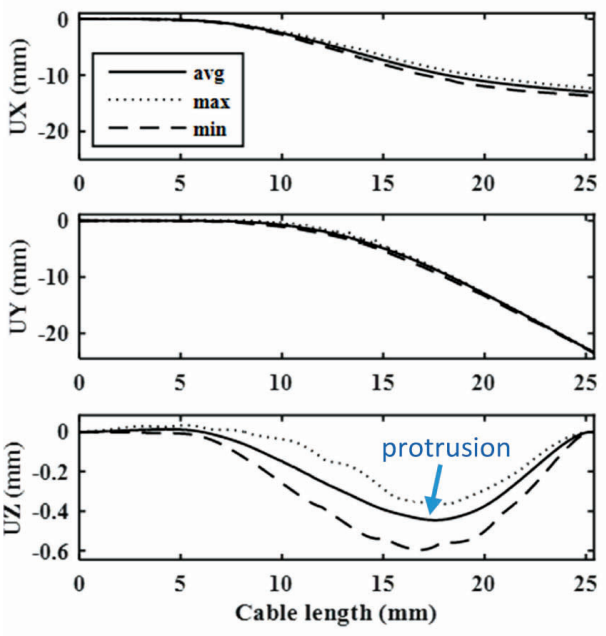

Fig. 18. Guide curve data interpretation (mm). Average, maximal and minimal strand displacement versus initial cable length

The strand pop-out instability is a local cable thickness alteration. The cable thickness is computed as a normal deviation from the winding path, which is shown in Fig. 19a as a dashed line.

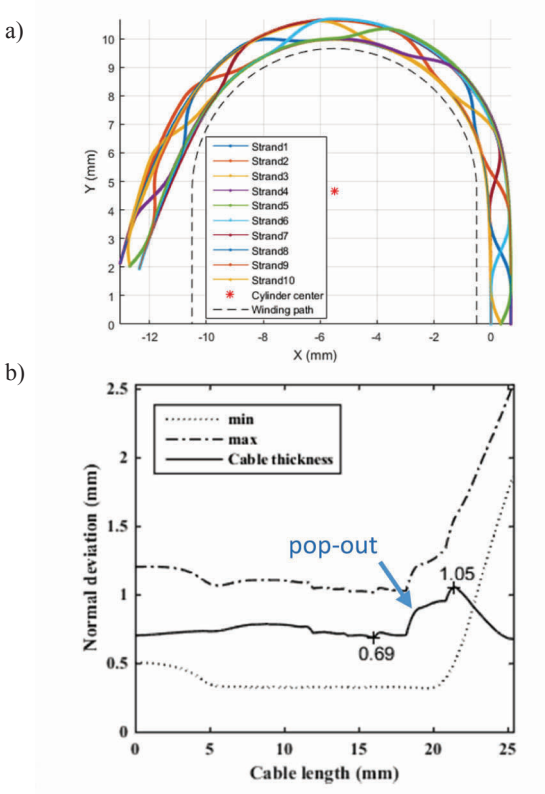

Fig. 19. Guide curve data interpretation (mm); a) Strand position with winding path; b) Cable normal deviation from winding path

The results in Fig. 19b show the cable thickness, maximum and minimum normal deviation of the cable from the winding path as a function of the cable length. One can see a marked minimal and maximal cable thickness at 16 mm and 21.4 mm of the winding path. The absolute difference equals 0.36 mm, which is 51% of a strand diameter.

Discussion and conclusion

The mechanical instability of a superconductor during winding is a present challenge in the magnet production process. The protrusion and the strand pop-out instabilities are observed during the prototype winding of 11 T and MQXF coils. It became important to study the winding process in a simulation environment in order to investigate the mechanical instabilities.

The FEA model of the winding process is presented. The material definition, the geometrical simplifications, and the boundary conditions are presented and discussed. The challenges of post-processing are addressed by the

guide curve analysis algorithm, which allows displaying the indicators of the protrusion and the strand pop-out as a function of the cable length.

The presented model and analysis method allows simulating the winding process, while paying special attention to the instabilities. Although the initial results are encouraging, the model requires further development aiming to increase the amount of strands and maintaining the simulation convergence time. This may be achieved by defining coarse mesh or simplifying boundary conditions.

References

1. Rossi L. and Bottura L., Superconducting Magnets for Particle Accelerators, Reviews of Accelerator Science and Technology, vol. 5, pp. 51–89, 2012.
2. Ferracin P., Ambrosio G., Anerella M., Borgnolutti F., Bossert R., Cheng D., Dietderich D.R., Felice H., Ghosh A., Godeke A., Bermudez S.I., Fessia P., Krave S., Juchno M., Perez J.C., Oberli L., Sabbi G., Todesco E., and Yu M., Magnet Design of the 150 mm Aperture Low-beta Quadrupoles for the High Luminosity LHC, IEEE Trans. Appl. Supercond., vol. 24, no. 3, pp. 1–6, 2014.
3. Karppinen M., Andreev N., Apollinari G., Auchmann B., Barzi E., Bossert R., Kashikhin V.V., Nobrega A., Novitski I., Rossi L., Smekens D., and Zlobin A.V., Design of 11 T twin-aperture Nb_3Sn dipole demonstrator magnet for LHC upgrades, IEEE Trans. Appl. Supercond., vol. 22, no. 3, pp. 3–6, 2012.
4. Cheggour N., Goodrich L.F., Stauffer T.C., Splett J.D., Lu X.F., Ghosh A.K., and Ambrosio G., Influence of Ti and Ta doping on the irreversible strain limit of ternary Nb_3Sn superconducting wires made by the restacked-rod process, vol. 23, no. 5, 2010.
5. Lackner F., Bourcey N., Ferracin P., Jozwiak P., Ohnweiler T., Revilak P., Savary F., and Triquet S., Analysis of Temperature Uniformity During Heat Treatment of Nb_3Sn Coils for the High-Luminosity LHC Superconducting Magnets, IEEE Trans. Appiled Supercond., vol. 26, no. 4, 2016.
6. Roy S.S., Potluri P., Canfer S., and Elwood G., Braiding Ultrathin Layer for Insulation of Superconducting Rutherford Cables, Journal of Industrial Textiles, 2016.
7. Pulikowski D., Lackner F., Scheuerlein C., Meinel D., Savary F., Tommasini D., and Pajor M., Testing Mechanical Behavior of Nb3Sn Rutherford Cable During Coil Winding, IEEE Trans. Appl. Supercond., vol. 27, no. 4, 2017.
8. Manil P., Mouzouri M., and Nunio F., Mechanical Modeling of Low Temperature Superconducting Cables at the Strand Level, IEEE Trans. Appl. Supercond., vol. 22, no. 3, 2012.
9. Arbelaez D., Prestemon S.O., Ferracin P., Godeke A., Dietderich D.R., and Sabbi G., Cable deformation simulation and a hierarchical framework for Nb_3Sn Rutherford cables, J. Phys. Conf. Ser., vol. 234, no. 2, 2010.
10. Cabanes J., Garlasche M., Bordini B., and Dallocchio A., Simulation of the cabling process for Rutherford cables: An advanced finite element model, Cryogenics (Guildf)., vol. 80, no. 3, 2016.
11. "ANSYS® Academic Research, Release 17.1, Help System, Mechanical™, ANSYS, Inc."